JOURNAL OF THERMOPHYSICS AND HEAT TRANSFER
Vol. 16, No. 1, January–March 2002

Stokes Flow Induced by a Sliding Smooth Plate over a Finned Plate

Jun Sang Park*
Halla University, Kangwondo 220-712, Republic of Korea
and
Jae Min Hyun†
Korea Advanced Institute of Science and Technology, Taejon 305-701, Republic of Korea

Slow viscous flow between a sliding smooth plate and a finned plate is investigated in the Stokes limit. Theoretical solutions are obtained for unidirectional flow along the fin. An exact analogy is noted between the present Stokes flow and the heat conduction under the same geometry. Conformal mapping is displayed to secure closed-form solutions to the case of single fin. For periodically spaced fins the eigenfunction expansion technique is utilized to describe the flow details. The explicit effects of the fin height and of the fin spacing on global flow patterns are elucidated. To gauge the increase in drag and heat transfer caused by the fin spacing, the concepts of fin-interaction parameter and characteristic length scales are introduced. The theoretical predictions and full-dress numerical solutions are shown to be highly consistent. Criteria for enhanced conductive heat transfer in microsystems are suggested.

Nomenclature

B^*	=	dimensional distance between the top and bottom plates
CL	=	characteristic length scale for fin interaction
D^*	=	dimensional fin-to-fin distance
d	=	nondimensional fin-to-fin distance
F	=	fin-interaction parameter
H^*	=	dimensional fin height
h	=	nondimensional fin height
S_1	=	physical variable ($\equiv x + iy$)
S_2	=	transformed variable ($\equiv x_1 + iy_1$)
W_0^*	=	dimensional velocity of the upper plate
w	=	velocity component in the z direction
x	=	horizontally cross coordinate
y	=	vertical coordinate
z	=	horizontally longitudinal coordinate
ζ	=	transformed variable ($\xi + i\eta$)
$\bar{\tau}$	=	average drag

I. Introduction

A THEORETICAL study is conducted to describe the slow motion of a viscous fluid induced by the sliding of a smooth plate over a plate with periodically spaced fins. In the present analysis the gap between the two plates is very small. Therefore, the relevant Reynolds number is sufficiently low that the inertia terms in the Navier–Stokes equations are ignored, which leads to the Stokes flow limit. The flow is generated by the sliding of the smooth plate along the fins. The geometrical layout, together with the coordinates, is sketched in Fig. 1.

The technological applications of the present flow are found in micromaching devices, Labyrinth sealing problems, and rotating shafts in electronic cooling situations, to name a few [e.g., Schey,[1] Patankar and Murthy,[2] Tai and Muller,[3] Wang[4]]. Especially in lubrication engineering a reduction of friction is achieved by entrapping lubricating oil in the grooves, which are produced in the turning or milling process.

Taylor[5,6] proposed the paint-brush model to depict the flow of paint between individual hair strands of the brush. This model flow resembles the present problem in the limit of spatially periodic fins of infinite height and negligible thickness. Justifications for this important theoretical model were provided. The work of Taylor[5,6] was extended by Richardson,[7] who utilized Schwarz–Christoffel mapping techniques, for the fins of infinite height and finite thickness. The drag experienced by the sliding plate was estimated, and he put forward theoretical grounds to develop pertinent boundary conditions for porous media.

The Stokes drag at the sliding plate was determined by Wang[4] by using an eigenfunction expansion and collocation method. Also, representative plots of the parallel flow were given. However, partially because of the limitations of the methodologies adopted the explicit effects of fin height and fin-to-fin spacing on significant flow variables were not delineated in detail. In particular, the intriguing aspects of cross interactions of the fins on the flow confined between two neighboring fins were not scrutinized in the previous investigations. In the present paper the influence of fin height and fin-to-fin spacing on the flow and drag characteristics is theoretically examined. Quantitative evaluations will be made of flow details, and the theoretical results will be compared with the full-dress numerical solutions.

From the governing equations it is of interest to note that analogy exists between the present problem and the heat conduction between the sliding smooth plate and the finned plate. Based on this analogy, the characteristic length scale for interfin interactions was derived. When the fin-to-fin spacing is smaller than this characteristic length, interfin interactions are shown to intensify.

The present theoretical findings will have ramifications in broad areas of industrial applications. One example is to secure a basis in the determination of fin pitch in Labyrinth seal or lubrication practices. These studies will be useful in establishing fundamental concepts of engineering roughness in flow between two plates.

Another closely related application can be found in drag reduction in turbulent boundary layer by employing longitudinal rib arrangements. Recent studies report drag reduction in the viscous sublayer, which can be modeled as a Stokes flow, under the assumption that the fluid extends to infinity over the wall with longitudinal rib

Received 23 January 2001; revision received 13 July 2001; accepted for publication 20 July 2001.

*Assistant Professor, Department of Mechanical Engineering, San 66, HeungUp, Wonju.
†Professor, Department of Mechanical Engineering, 373-1 Kusong-Dong, Yusung-gu.

arrangement. This configuration is similar to the present problem in which the sliding upper plate is absent.[8–10] The Stokes flow of a Newtonian fluid in a channel, bounded by a flat plate on one side and by a fractal porous medium on the other one, has been studied by Vignes-Adler et al.[11]

II. Model

Consider the two-dimensional flow of a viscous fluid [density ρ^*, kinematic viscosity ν^*] in the gap between the sliding smooth upper plate ($y^* = B^*$) and the stationary bottom plate ($y^* = 0$). An array of periodically located vertical fins of height H^* and of negligible thickness are attached to the bottom plate. The fin-to-fin distance (fin pitch) is defined as D^*. The flow is maintained by the sliding motion of the upper plate in the z^* direction with W_0^*, as sketched in Fig. 1a.

In the Stokes limit the nondimensionalized governing equations for the velocity w in the z direction are (e.g., Wang[4])

$$\frac{\partial^2 w}{\partial x^2} + \frac{\partial^2 w}{\partial y^2} = 0 \tag{1}$$

under the nondimensionalization scheme

$$d = D^*/B^*, \qquad h = H^*/B^*, \qquad w = w^*/W_0^*$$

$$(x,\ y) = (x^*/B^*,\ y^*/B^*)$$

with an asterisk indicating dimensional quantities.

Because the problem is symmetric about the centerline ($x = d/2$), the associated boundary conditions are

$$w = 1 \quad \text{at} \quad 0 \le x \le d/2,\ y = 1 \tag{2}$$

$$w = 0 \quad \text{at} \quad 0 \le x \le d/2,\ y = 0 \tag{3}$$

$$w = 0 \quad \text{at} \quad x = 0,\ 0 \le y \le h \tag{4}$$

$$\frac{\partial w}{\partial x} = 0 \quad \text{at} \quad x = 0,\ h \le y \le 1 \tag{5}$$

$$\frac{\partial w}{\partial x} = 0 \quad \text{at} \quad x = d/2,\ 0 \le y \le 1 \tag{6}$$

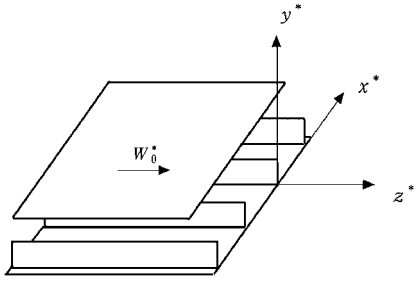

Fig. 1a Flow layout.

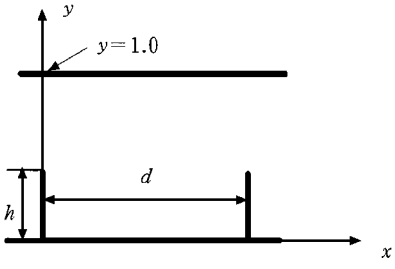

Fig. 1b Coordinate system.

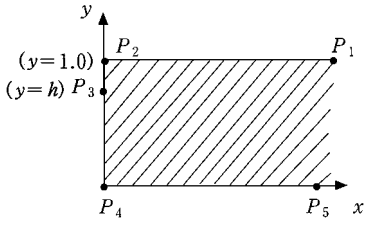

a) S_1-plane

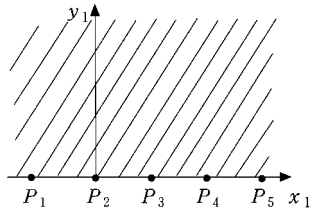

b) S_2-plane

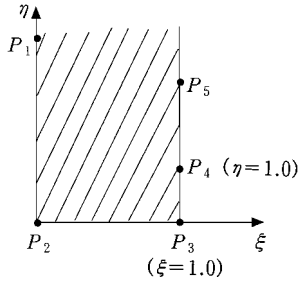

c) ζ-plane

Fig. 2 Schematics of conformal transformations.

III. Analysis

A. Single-Fin Model ($d \to \infty$)

First, attention is given to the case when there is only one fin at $x = 0$, that is, $d \to \infty$ in Fig. 1b. The problem is symmetric with respect to the y axis. As displayed in Fig. 2a, it is advantageous to consider in the $S_1 (\equiv x + iy)$ plane the semi-infinite region, which is defined by $\overline{P_1P_2}$, $\overline{P_2P_3}$, $\overline{P_3P_4}$, and $\overline{P_4P_5}$.

By using the Schwarz–Christoffel transformation, the S_1 plane is mapped into the $S_2 (\equiv x_1 + iy_1)$ plane (Fig. 2b):

$$\frac{dS_1}{dS_2} = A(S_2 - \gamma_1)^{-\frac{1}{2}}(S_2 - \gamma_2)^{-\frac{1}{2}} \tag{7}$$

In the preceding, γ_i indicates the point in the S_2 plane corresponding to the point P_i in the S_1 plane.

Setting $\gamma_1 = 0$ and $\gamma_2 = \lambda$, Eq. (7) yields

$$S_1 = A\int_0^{S_2} \omega^{-\frac{1}{2}}(\omega - \lambda)^{-\frac{1}{2}}\, d\omega + B \tag{8}$$

The transformation from the S_2 plane to the $\zeta (\equiv \xi + i\eta)$ plane is made by using (Fig. 2c)

$$S_2 = \sin^2(\pi\zeta/2) \tag{9}$$

The undetermined constants A, B, and λ in Eq. (8) can be determined by using the condition that the three points (0, 1), (0, h), and (0, 0) in the S_1 plane be mapped onto (0, 0), (1, 0), and (λ, 0) in the S_2 plane, that is,

$$A = \frac{1 - h}{\int_0^1 \omega^{-\frac{1}{2}}(\lambda - \omega)^{-\frac{1}{2}}\, d\omega} \tag{10}$$

$$B = i\left(\equiv \sqrt{-1}\right) \tag{11}$$

$$\int_1^\lambda \omega^{-\frac{1}{2}}(\lambda - \omega)^{-\frac{1}{2}}\, d\omega = \frac{h}{1 - h}\int_0^1 \omega^{-\frac{1}{2}}(\lambda - \omega)^{-\frac{1}{2}}\, d\omega \tag{12}$$

In practice, λ is found from the integral equation (12), and by using the result in Eq. (10) A can be determined, that is,

$$\lambda = 1/\sin^2[(\pi/2)(1-h)] \tag{13}$$

$$A = 1/\pi \tag{14}$$

Combining the foregoing developments, the transformation formula from the S_1 plane to the ζ plane is obtained:

$$S_1 = -i\int_0^{\zeta}\left\{\frac{\sin^{-2}[(\pi/2)(1-h)] - \sin^2(\pi\omega/2)}{\cos^2(\pi\omega/2)}\right\}^{-\frac{1}{2}} d\omega + i \tag{15}$$

and, the result of integration of Eq. (15) gives

$$\zeta = (2/\pi)\sin^{-1}\left[\sqrt{\lambda}\cdot\sin(\pi/2)(1-iS_1)\right] \tag{16}$$

By using the preceding conformal transformation, the governing equation in the ζ plane remains to be the Laplace equation (e.g., Ahlfors[12]):

$$\frac{\partial^2 w}{\partial\xi^2} + \frac{\partial^2 w}{\partial\eta^2} = 0 \tag{17}$$

with the boundary conditions

$$w = 1 \quad \text{at} \quad \xi = 0 \tag{18}$$

$$w = 0 \quad \text{at} \quad \xi = 1 \tag{19}$$

$$\frac{\partial w}{\partial\eta} = 0 \quad \text{at} \quad \eta = 0 \tag{20}$$

in which $\xi = 0$ denotes the upper plate surface, $\xi = 1$ the lower fin and plate surfaces, and $\eta = 0$ the central symmetric plane, that is, $x = 0$ in the physical domain.

The solution to the preceding equation is readily found:

$$w(\xi,\eta) = 1 - \xi \equiv \text{Real part of}\,(1-\zeta) \tag{21}$$

From Eqs. (16) and (21), the isovelocity lines in the S_1 plane are described by the curves

$$\frac{\cosh^2(\pi x/2)\cos^2(\pi y/2)}{C_1} - \frac{\sinh^2(\pi x/2)\sin^2(\pi y/2)}{1-C_1} = \sin^2\left[\frac{\pi}{2}(1-h)\right] \tag{22}$$

in which $C_1 \equiv \sin^2(\pi\xi/2)$.

Numerical solutions to Eq. (22) illustrate the isolines of w velocity in the vicinity of the fin (Fig. 3). Clearly, as h increases the isovelocity lines are clustered near the fin apex. This points to steep velocity gradients in the fin apex region, which contributes to an increase of the local friction coefficient. It is also discernible that as h increases the global patterns of isovelocity lines are more crowded closer to the upper plate, which indicates an increase in drag experienced by the upper plate. As is obvious in Fig. 3a, when h is small the influence of the fin on the flow near the upper plate is minimal.

The flow behavior far away from the fin is of interest. By setting $x \to \infty$ in Eq. (22) produces

$$\cos[\pi(y-\xi)/2]\cdot\cos[\pi(y+\xi)/2] = 0 \tag{23}$$

for $0 \le y \le 1$ and $0 \le \xi \le 1$. To maintain Eq. (23) for arbitrary values of ξ (within the range $0 \le \xi \le 1$), it is seen that

$$\cos[\pi(y+\xi)/2] = 0, \qquad \text{i.e.,} \qquad y = 1-\xi$$

The preceding, together with Eq. (21), leads to

$$w(x\to\infty, y) = y \tag{24}$$

which, as expected, recovers the standard Couette flow between two parallel plates with gap distance 1. This exercise serves also as a test of the validity of the present theoretical approaches.

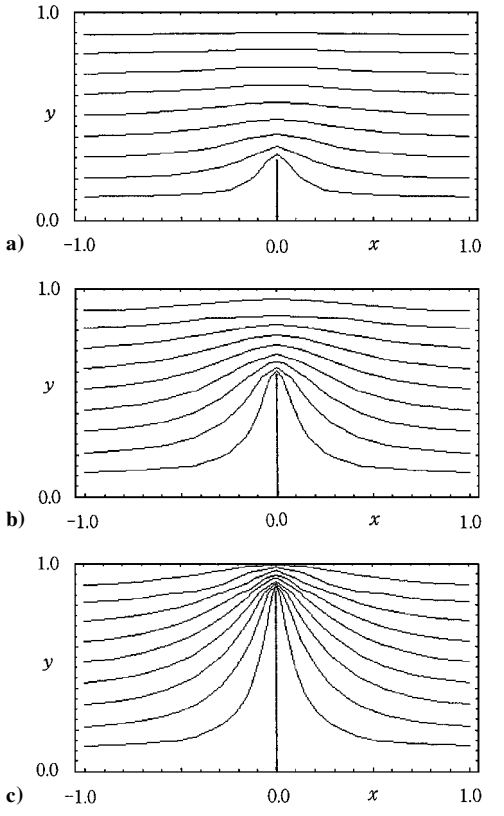

Fig. 3 Plots of isovelocity w lines for the single-fin model ($d \to \infty$). Values of h are a) 0.3, b) 0.6, and c) 0.9. The contour increment is 0.1.

B. Periodically Placed Fins (d Finite)

When the fin pitch d is finite, analytical solutions to Eq. (1) are difficult to construct. Following Wang,[4] the eigenfunction expansion technique will be deployed.

The solution for w in Eq. (1) is assumed to be of the form $(0 \le x \le d/2, 0 \le y \le 1)$

$$w(x,y) = y + \sum_{n=1}^{\infty} A_n \sin(n\pi y)\left[e^{n\pi(x-d)} + e^{-n\pi x}\right] \tag{25}$$

where A_n are coefficients to be determined. Equation (25) satisfies all of the boundary conditions except the one at $x = 0$. Introducing the boundary conditions at $x = 0$, that is, $w(x=0, 0 \le y \le h) = 0$, $w_x(x=0, h \le y \le 1) = 0$, into Eq. (1) yields

$$y + \sum_{n=1}^{\infty} A_n \sin(n\pi y)(e^{-n\pi d} + 1) = 0, \qquad (0 \le y \le h) \tag{26}$$

$$\sum_{n=1}^{\infty} n\pi A_n \sin(n\pi y)(e^{-n\pi d} - 1) = 0, \qquad (h \le y \le 1) \tag{27}$$

The infinite series are truncated to N terms, and the resulting linear equations are obtained:

$$y_i + \sum_{n=1}^{M} A_n \sin(n\pi y_i)(e^{-n\pi d} + 1) = 0$$

$$(0 \le y_i \le h), \quad i = 1, 2, \ldots, M$$

$$\sum_{n=M+1}^{N} n\pi \sin(n\pi y_i)(e^{-n\pi d} - 1) = 0$$

$$(h \le y_i \le 1), \quad i = M+1, M+2, \ldots, N$$

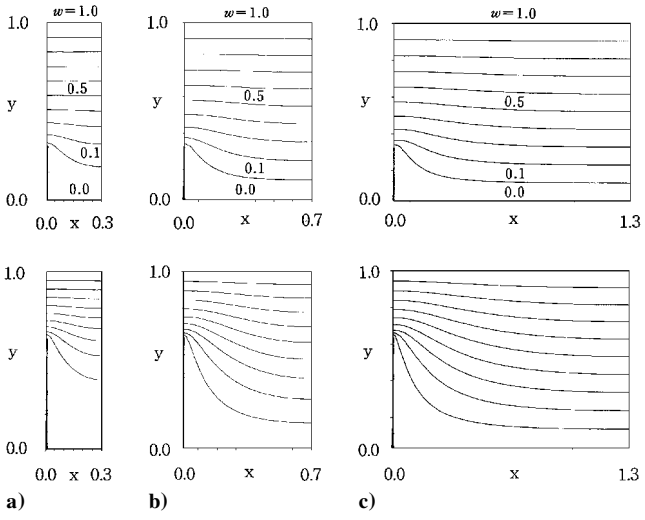

Fig. 4 Plots of isovelocity w lines for the periodic-fin model ($d \rightarrow$ finite). Values of the fin-to-fin distance d are a) 0.6, b) 1.4, and c) 2.6. $h = 0.33$ (top frames), and $h = 0.66$ (bottom frames). The contour increment is 0.1. In the plots only the left half of the whole domain is shown ($0 \le x \le d/2$).

As remarked by Wang,[4] when y_i are equally spaced the error of the present approximations falls below 1% when $N = 60$. In the present calculations N was set 100.

After the coefficients A_n are determined by the preceding approximate matrix inversion method with Gauss elimination, the average drag at the upper plate ($y = 1$) can be evaluated

$$\bar{\tau}\left(\equiv \frac{\tau^*}{\mu^* W_0^* / D^*} \right) = \frac{2}{d} \int_0^{d/2} \frac{\partial w(x,1)}{\partial y}\, \mathrm{d}x$$

$$= 1 + \frac{2}{d} \sum_{n=1}^{N} (-1)^n A_n (1 - e^{-n\pi d}) \tag{28}$$

Exemplary solutions for isolines of w velocity are exhibited in Fig. 4 for varying values of h and d. It is discernible that as h increases the overall flows tend to be shifted closer to the upper plate, which is akin to the case of a single fin. This trend is more pronounced as the fin pitch d decreases. In summary, the velocity gradients near the upper plate increase, which gives rise to an increase in drag, as h increases or d decreases. The y profile of velocity at the centerline ($x = d/2$) is informative. When d is large (Fig. 4c), this y profile is substantially describable by that of Couette flow, that is, $w = y$. On the other hand, when d is small (Fig. 4a), this y profile deviates considerably from that of Couette flow. In the limit of $d \rightarrow 0$, it can be easily predicted that the flow occurs between two parallel plates with a gap of $(1 - h)$. It follows that the explicit effect of d can be assessed by evaluating the degree of departure of the velocity profile at the centerline ($x = d/2$) from that of a Couette flow, that is, $w = y$.

IV. Fin-to-Fin Interactions

In an effort to quantify the effect of finite d on the resulting flow and drag, the aforestated two limiting situations are considered. When $d \rightarrow \infty$, the flow at the centerline ($x = d/2$) is unaffected by the presence of fins and, therefore, is depicted by the Couette flow, that is,

$$\lim_{d \rightarrow \infty} \{w(x = d/2, y)\} = y \tag{29}$$

In the opposite case, when $d \rightarrow 0$ the centerline flow approaches the Couette flow with a gap $(1 - h)$, that is,

$$\lim_{d \rightarrow 0} \{w(x = d/2, y)\} = (y - h) \cdot H(y - h) \tag{30}$$

in which H denotes the Heaviside unit step function.

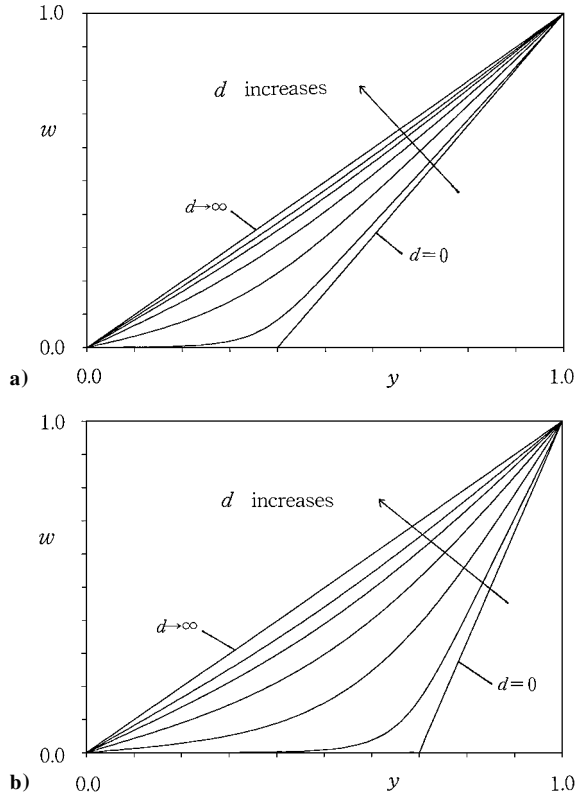

Fig. 5 The y profiles of w at the centerline $x = d/2$. Values of d for the curves are 0, 0.2, 0.6, 1.0, 1.4, 1.8, ∞ . Values of h are a) 0.4 and b) 0.7.

Figure 5 portrays the y profile of w velocity at the centerline ($x = d/2$). It is obvious that the just stated two limiting cases are shown in straight lines, and the flows for finite d are indicated by the curves between these two lines.

As emphasized earlier, the direct effect of fins can be appraised by quantitatively measuring the degree of departure of the centerline flow profile from that of the standard Couette flow ($d \rightarrow \infty$), that is,

$$F(d,h) = 2 \int_0^1 \left| y - w\left(x = \frac{d}{2}, y \right) \right| \mathrm{d}y \tag{31}$$

In Eq. (31), $F(d,h)$ represents the normalized effect of fin-to-fin interactions as a result of the finiteness of fin pitch. In Fig. 5 F denotes twice the area bounded by the straight line of the standard Couette flow, linking points (0,0) and (1,1), and by the w curve.

The usefulness of F is illustrated in Fig. 6. As already stressed, the fin-to-fin interactions increase as h increases and d decreases. The plots confirm the earlier assertion that, in the limit $d \rightarrow \infty$, F tends to zero, which indicates that the flow approaches the standard Couette flow $w = y$.

To quantify the strength of fin-to-fin interactions, it will be desirable to define a length scale, which characterizes the effect of finite fin spacing.

For this purpose it is noted that an exact analogy exists between the present unidirectional Stokes flow and the problem of heat conduction between the upper plate (at constant temperature T_T) and the periodically placed fins and lower plate (at constant temperature T_B). The isovelocity lines of Eq. (20) correspond to the isotherms of heat-conduction problem. By using this analogy, physical interpretations can be had by resorting to more physically accessible concepts.

As stipulated in Sec. III.A, for the case of a single fin the isotherms in the ζ plane are given by $\xi = \text{const}$. Consequently, the heat-flux lines, which are perpendicular to the isotherms, in the ζ plane are depicted by $\eta = \text{const}$. Because the transformation equation (14) is based on conformal mapping, the heat-flux lines in the physical plane can be found by simple manipulations:

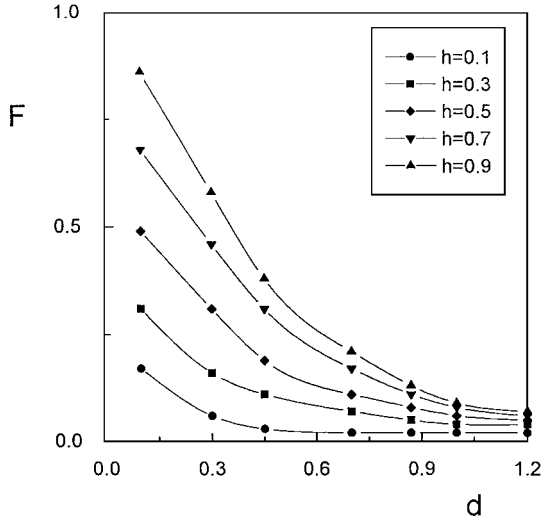

Fig. 6 Fin-interaction parameter F [Eq. (31)].

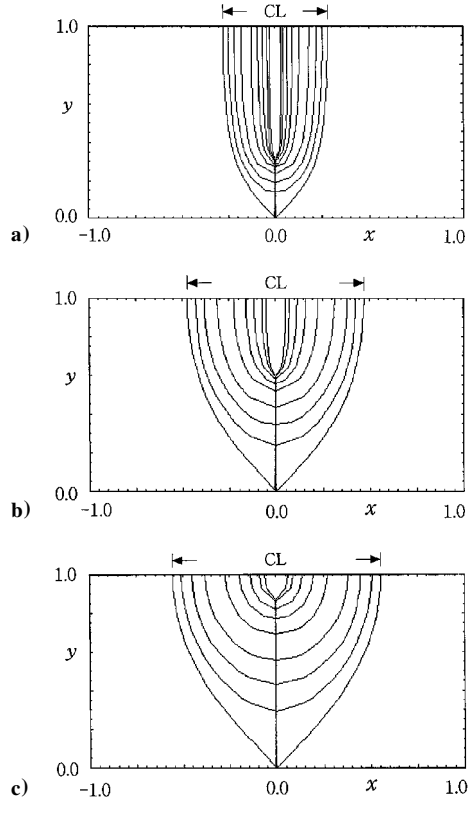

Fig. 7 Plots of heat-flux lines from a single fin model ($d \to \infty$). Values of h are a) 0.3, b) 0.6, and c) 0.9.

$$\frac{\cosh^2(\pi x/2)\cos^2(\pi y/2)}{1+C_2} + \frac{\sinh^2(\pi x/2)\sin^2(\pi y/2)}{C_2} = \sin^2\left[\frac{\pi}{2}(1-h)\right] \tag{32}$$

where $C_2 \equiv \sinh^2(\pi\eta/2) \geq 0$.

The heat-flux lines from a single fin (excluding the bottom plate) as computed from Eq. (32), are plotted in Fig. 7. Clearly, the heat-flux lines, originating from the fin, spread out toward the upper plate. The width shown as CL at the upper plate, which is marked by the heat-flux line coming from the bottom of the fin, characterizes the zone of influence of the single fin.

In Fig. 7, as h increases CL increases, which implies that the area of the upper plate under direct influence of the fin widens.

By utilizing the foregoing results for the single-fin model, a theoretical solution for CL will be derived. As mentioned, by virtue of the analogy between the present flow and the heat-conduction problem CL will signify the characteristic length to measure the effect of fin-to-fin interactions in the determination of drag.

The heat-flux line from the bottom of the fin can be found by setting $x = 0$, $y = 0$ in Eq. (32), which gives

$$C_2 = 1/\cos^2(\pi h/2) - 1$$

The x coordinate of this heat-flux line at the upper plate ($y = 1$) is readily available:

$$x = (2/\pi)\sinh^{-1}[\sin(\pi h/2)] \tag{33}$$

The characteristic length CL at the upper plate for a single fin can be defined to be twice of this x coordinate, that is,

$$CL = (4/\pi)\sinh^{-1}[\sin(\pi h/2)] \tag{34}$$

Now, consider an array of periodically spaced fins. If the fin pitch d is smaller than CL, the heat-flux lines from the adjacent fins meet each other. This interaction between the fins pushes the isotherms (or isovelocity lines) toward the upper plate in comparison to the case of an uninterfered single fin (see Fig. 4a and Fig. 7). The result is that the isotherms (or isovelocity lines) are crowded in the vicinity of the upper plate, which brings forth an enhancement of heat transfer (or an increase in drag) at the upper plate. On the contrary, when $d > CL$ the heat- flux lines from the neighboring fins do not overlap. Consequently, the solutions for periodic fins approach the solution for a single fin (Fig. 4c).

Figure 8 exhibits the results of full-dress numerical computations of the governing equations for heat conduction for multifin arrays. These are highly consistent with the preceding theoretical solutions to the single-fin model. As d decreases or h increases, the heat-flux lines are clustered toward the fin.

Figure 9 illustrates the theoretical values of CL [Eq. (34)], together with the full-scale computational data for CL for the case of $F = 0.1$. It is discernible that these two sets of solutions are in satisfactory agreement. These favorable comparisons of data provide support to the consistency of the concepts of F, that is, the degree of departure from the standard Couette flow, and of CL, that is, the area engulfed by the heat-flux lines from the fins. The value of CL of theoretical prediction is slightly higher than the computational result as h increases. The heat-flux lines in the single-fin model disperse to a wider area in the horizontal direction because there is no fin interaction than in the case of fin-array model. It is

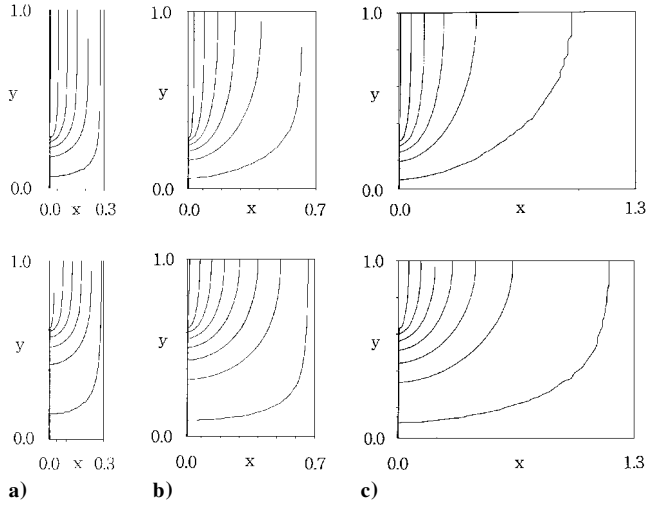

Fig. 8 Plots of heat-flux lines from periodic-fin arrays ($d \to$ finite). Only the left half ($0 \leq x \leq d/2$) is shown. Values of d are a) 0.6, b) 1.4, and c) 2.6. Values of h are $h = 0.33$ (top frames), and $h = 0.66$ (bottom frames).

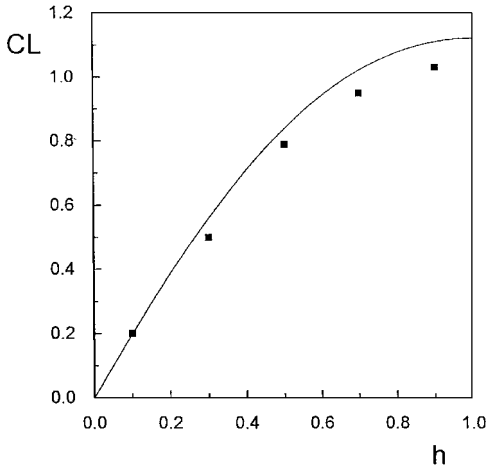

Fig. 9 Characteristic length scale *CL*: ——, theoretical solution, Eq. (34); and ■, numerical solution for $F = 0.1$.

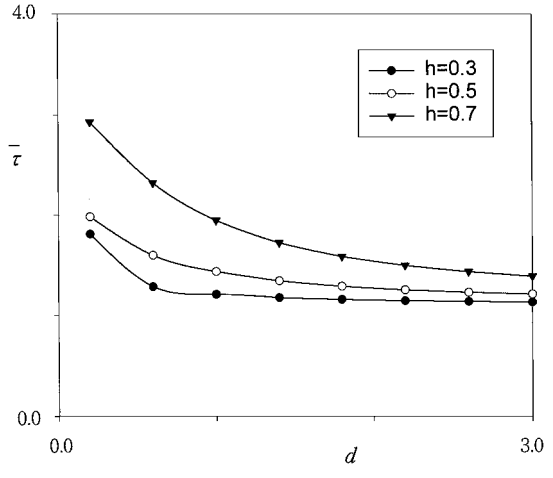

Fig. 10 Average drag $\bar{\tau}$ at the upper plate ($y = 1$).

recalled that the analytical prediction is for the single-fin model, and the numerical result is for the fin-array model.

The average drag at the upper plate, that is,

$$\bar{\tau} = \frac{1}{d}\int_0^d \frac{\partial w(x, y=1)}{\partial y}\,\mathrm{d}x \tag{35}$$

is plotted in Fig. 10. Evidently, $\bar{\tau}$ increases as d decreases or h increases. The results in Fig. 10 are in line with the preceding assertions involving CL, which reinforces the usefulness of the concepts of CL and F.

V. Conclusions

Slow viscous flow between a sliding smooth plate and a finned plate is studied in the Stokes limit.

Theoretical solutions are obtained for unidirectional flow along the fin. Velocity fields are computed for a single fin by setting the fin pitch $d \to \infty$. For the case of finite d, the eigenfunction expansion method is deployed. The interaction between two neighboring fins is delineated. The drag increase on the sliding smooth plate is noted.

Based on the precise analogy between the flow and the heat conduction in the same geometry, the interaction parameter F and the characteristic length scale CL are introduced. Favorable comparisons between the present theoretical predictions and the full-dress numerical solutions underscore the usefulness of the concepts involving F and CL in ascertaining the degree of fin-to-fin interactions.

Acknowledgment

This work was supported by Grant Number 2000-2-30500-003-5 from the Basic Research Program of the Korea Science and Engineering Foundation.

References

[1]Schey, J. A., *Tribology in Metalworking-Friction, Lubrication and Wear*, American Society for Metals, Metal Park, OH, 1983, pp. 2–10.

[2]Patankar, J. Y., and Murthy, S. V., "Analysis of Heat Transfer from a Rotating Cylinder with Circumferential Fins," *Heat and Mass Transfer in Rotating Machinery*, Hemisphere, New York, 1984, pp. 155–166.

[3]Tai, Y. C., and Muller, R. S., "IC-Processed Electrostatic Synchronous Micromotors," *Sensors and Actuators*, Vol. 20, 1989, pp. 49–56.

[4]Wang, C. Y., 'The Stokes Drag due to the Sliding of a Smooth Plate over a Finned Plate," *Physics of Fluids*, Vol. 6, No. 7, 1994, pp. 2248–2252.

[5]Taylor, G. I., "Deposition of a Viscous Fluid on a Plane Surface," *Journal of Fluid Mechanics*, Vol. 9, 1960, pp. 218–225.

[6]Taylor, G. I., "A Model for the Boundary Condition of a Porous Material. Part 1," *Journal of Fluid Mechanics*, Vol. 49, 1971, pp. 319–326.

[7]Richardson, S., "A Model for the Boundary Condition of a Porous Material. Part 2," *Journal of Fluid Mechanics*, Vol. 49, 1971, pp. 327–336.

[8]Bechert, D. W., and Bartenwerfer, M., "The Viscous Flow on Surfaces with Longitudinal Ribs," *Journal of Fluid Mechanics*, Vol. 206, 1989, pp. 105–129.

[9]Luchini, P., Manzo, F., and Pozzi, A., "Resistance of a Grooved Surface to Parallel Flow and Cross-Flow," *Journal of Fluid Mechanics*, Vol. 228, 1991, pp. 87–109.

[10]Pozrikidis, C., "Unsteady Viscous Flow over Irregular Boundaries," *Journal of Fluid Mechanics*, Vol. 255, 1993, pp. 11–34.

[11]Vignes-Adler, M., Adler, P. M., and Gougat, P., "Transport Process Along Fractals. The Cantor-Taylor Brush," *PhysicoChemical Hydrodynamics*, Vol. 8, 1987, pp. 401–422.

[12]Ahlfors, L. V., *Complex Analysis*, McGraw–Hill, New York, 1979, pp. 229–235.